Optical Materials 180 (2026) 118434

Contents lists available at ScienceDirect

Optical Materials

journal homepage: www.elsevier.com/locate/optmat

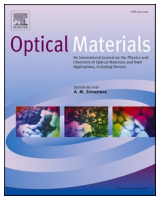

Porous silica coatings for radiative cooling and anti-reflection for enhancing solar photovoltaics performance

Leonard E. Namwiha [a,b], Markus Guttmann [a], Marco Ehrhardt [a], Tonghan Zhao [a], Bryce S. Richards [a,c,*], Gan Huang [a,**]

[a] Institute of Microstructure Technology, Karlsruhe Institute of Technology, Hermann-von-Helmholtz-Platz 1, Eggenstein-Leopoldshafen, D-76344, Germany
[b] Department of Physics, Chemistry and Material Science, University of Namibia, Private Bag 13301, Windhoek, Namibia
[c] Light Technology Institute, Karlsruhe Institute of Technology, Engesserstrasse 13, Karlsruhe, D-76131, Germany

ARTICLE INFO

Keywords:
Porous silica
Sol-gel method
Anti-reflective coating
Radiative cooling
Transmittance
Emissivity

ABSTRACT

The cover glass of solar photovoltaic (PV) modules is known to suffer from reflectance losses, while elevated operating temperatures further reduce PV efficiency. This study investigates the application of porous silica coatings to reduce solar reflectance in the spectral range of 300–1200 nm and enhance thermal emissivity in the mid-infrared range of 8–13 μm. A sol-gel method employing a base/acid double-catalysis technique was used to synthesize a silicon dioxide (SiO_2) sol, which was subsequently spin-coated onto glass substrates to form porous silica layers. The materials and optical properties of the coatings were characterised using scanning electron microscopy, Fourier transform infrared spectroscopy, and spectrophotometry. A two-layer design demonstrates a 1.2% absolute increase in solar transmittance (300–1200 nm) with a porous silica layer, along with an enhancement in mid-infrared emissivity (8–13 μm) from 87% to 90%, compared to bare glass. A three-layer configuration increases the emissivity to 96%, but with a 1.1% absolute reduction in transmittance within the 300–1200 nm range.

1. Introduction

Two key challenges that affect photovoltaic (PV) module performance are optical reflection losses from the front side of the cover glass and reduced electrical output due to elevated operating temperatures [1]. At the air-glass interface, reflection losses can account for ~5% of the incident solar radiation, depending on the deviation of the angle of incidence. These losses decrease the amount of light absorbed by the solar cells, limiting the generation of electron-hole pairs and thus reducing overall power output [2].

Typically, a modern silicon-based PV module is rated with a power conversion efficiency of 22–24% when tested under standard test conditions (STC), which means under 1000 W/m^2 intensity of the air-mass 1.5 global (AM1.5G) solar spectrum and, most importantly, operating at 25 °C. This means that more than 70% of sunlight contributes to heat build-up, raising the PV module's operating temperature to 60 – 80 °C on summer days [3]. For every 1 °C increase in operating temperature above its 25 °C rating, the power output of a silicon PV module declines by approximately 0.24% to 0.35% [4]. Therefore, among the broader range of strategies being studied to improve PV system performance, reducing front-surface reflection and enhancing waste heat dissipation are two important approaches [5,6].

To address these issues, various surface coatings and cooling techniques have been developed [7]. Typical anti-reflection coating structures include porous coating (e.g., porous silica [8]) and micro-structured coating (e.g., moth-eye-like structure [9], micro-pyramid structure [10], micro-cone structure [11] etc). Cooling strategies include active cooling, passive cooling, phase change materials (PCMs), and enhanced PCM methods with additives such as nanoparticles or porous metals [7,12]. Among these, passive daytime radiative cooling (PDRC) has gained significant recent attention [13,14]. PDRC materials exhibit high solar reflectance and strong mid-infrared (MIR) emissivity (8–13 μm), enabling them to dissipate heat to the cold sky without energy input. Compared to active cooling

This article is part of a special issue entitled: SHIFT 2025 published in Optical Materials.

* Corresponding author. Institute of Microstructure Technology, Karlsruhe Institute of Technology, Hermann-von-Helmholtz-Platz 1, D-76344, Eggenstein-Leopoldshafen, Germany.
** Corresponding author.
E-mail addresses: bryce.richards@kit.edu (B.S. Richards), gan.huang@kit.edu (G. Huang).

https://doi.org/10.1016/j.optmat.2026.118434
Received 8 April 2026; Received in revised form 21 July 2026; Accepted 17 August 2026
Available online 18 August 2026

systems, which consume additional energy, PDRC offers a more energy-efficient and sustainable solution [15]. Recent analysis shows that radiative cooling can increase the annual electricity yield of PV modules by ~3 rel.% [16].

Porous silicon dioxide (SiO_2), or silica, has been widely studied for optical coatings due to its low refractive index (~1.44), mechanical durability, and chemical resistance [2,17]. Its tuneable pore size and ability to form nanostructured coatings make it ideal for developing anti-reflective surfaces. Additionally, porous silica can effectively emit thermal radiation in the atmospheric transparency window (8-13 μm), helping to reduce PV module temperatures and thus enhance energy conversion efficiency [18]. The radiative cooling behaviour is primarily due to the vibrational modes of Si–O–Si bonds, which strongly interact with mid-infrared radiation [19]. Compared to bare glass, which also contains silica as a primary component, the porous silica coating can enhance thermal emission [20].

The sol-gel method is a cost-effective and versatile technique for synthesising silica nanoparticles used in optical coatings [21,22]. In the sol-gel process, alkoxysilane precursors such as tetraethyl orthosilicate (TEOS) and methyltriethoxysilane (MTES) are hydrolysed and condensed, typically in the presence of catalysts like hydrochloric acid (acidic) or ammonium hydroxide (basic) [22–24]. Acid catalysts promote hydrolysis and produce branched, adhesive structures, whereas base catalysts enhance condensation, yielding spherical nanoparticles that adhere less strongly to substrates [22,25]. A double-catalysis approach, combining acid and base catalysts, can produce scratch-resistant, high-quality porous coatings with low refractive indices [25]. The porosity of the silica coating, and hence its refractive index, can be tailored using agents like Pluronic F127, which create a more porous nanostructure [26,27]. The sol is then deposited on substrates via methods such as dip coating or spin coating. Spin coating is particularly preferred due to its precise control over coating thickness, uniformity, simplicity and easy to set up, making it ideal for research, although it is limited to small sample size up to 6 cm [28,29]. The sol's viscosity plays a key role in determining the coating thickness: higher viscosity results in thicker films, while lower viscosity yields thinner layers. For anti-reflective purposes, coating thicknesses lower than 200 nm are considered optimal to avoid scattering of light in the 300–1200 nm range.

While sol-gel porous silica coating has been applied to either anti-reflective [30,31] or radiative cooling [32,33], the dual functionality of sol-gel porous silica coatings, i.e., enhancing both light transmittance and radiative heat dissipation at the same time, remains underexplored. In the current literature, such combined performance for solar cells is mainly achieved using silica micro-grating coatings [34] or micro-pyramid coating [35].

This study aims to fabricate porous silica coatings with tailored pore sizes and porosity that offer simultaneous anti-reflective and radiative cooling performance. The coatings were sintered on the low-iron soda-lime glass (Fig. 1), acting as both anti-reflective layers and thermal emitters. The coatings are characterised in terms of transmittance, reflectance, and thermal emissivity. This work offers a pathway to higher energy yield for PV modules.

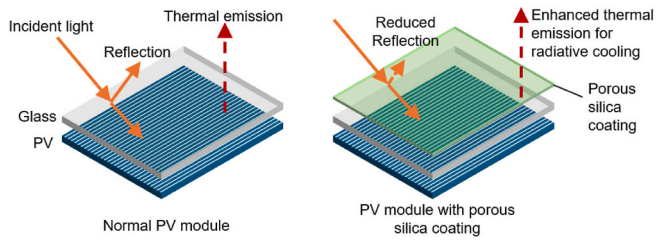

Fig. 1. The concept of porous silica coatings for radiative cooling and anti-reflection for enhancing PV module performance.

2. Experimental methods

2.1. Materials preparation

Tetraethyl orthosilicate (TEOS) (99.9%) purchased from VWR (Germany) was used as the precursor for the synthesis of SiO_2 coatings. Ammonium hydroxide served as the base catalyst, while 0.1 M hydrochloric acid was used as the acid catalyst. The triblock copolymer Pluronic F127 (99.9%), purchased from VWR (Germany), functioned as a surfactant to enhance porosity. Ethanol (99.9%) was employed as the solvent. All chemicals were used as received, without further purification. Prior to experimentation, all containers and apparatus were thoroughly cleaned with ethanol, rinsed with deionised water, and dried.

2.2. Chemical process and coating fabrication

In this study, three silica sols were synthesised using a sol-gel method based on a base/acid double-catalysis process. This method involves the preparation of two separate sols: one catalysed with hydrochloric acid (acid-catalysed) and the other with ammonium hydroxide (base-catalysed) [36,37]. After individual preparation, the two sols were combined and aged for 24 h prior to spin coating. The sols were prepared in two parts, referred to as Part A and Part B. The base-catalysed sol (Part A) was prepared using approximately 150 mL total volume of TEOS, ethanol, and distilled water in the ratio of 20 : 115: 8 mL, respectively. Ammonium hydroxide was added dropwise to act as the base catalyst. The experimental setup consisted of a 250 mL three-neck round-bottom flask: the central neck was connected to a water-cooled condenser, while one of the remaining openings was used for reagent addition and pH measurement, and the third housed a thermometer for real-time temperature monitoring.

As illustrated in Fig. 2, 20 mL of TEOS was first added into the flask, followed by 115 mL of ethanol. The mixture was stirred at room temperature for 5 min using a magnetic stirrer. Subsequently, the solution was heated to 60 °C, and 8 mL of distilled water was added. While stirring, 5 mL of ammonium hydroxide was added dropwise until the pH reached 10. The mixture was then stirred at 60 °C for 90 min. During this stage, a colour change from clear to bluish-white was observed, likely indicating nanoparticle formation via condensation and light scattering [38]. The sol was then transferred to an oven and aged for 3 h at 35 °C, to stabilise the sol. It was later returned to the flask and heated to 86 °C for reflux. The steady reflux temperature was observed to be 76 °C. Reflux was maintained for approximately 7 h until the pH dropped to 7, ensuring ammonia evaporation. This step is critical as residual ammonia can adversely affect the final coating properties [39].

The acid-catalysed sol (Part B) was then prepared. The volume ratio of TEOS: ethanol: water was 5 : 80: 3 (mL). Initially, 77 mL of ethanol and 3 mL of distilled water were added into a 250 mL beaker and stirred

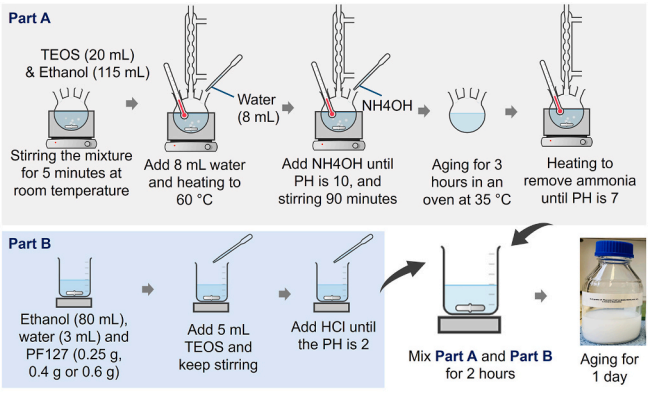

Fig. 2. Schematic illustration of the sol-gel synthesis process (Part A and Part B).

with a magnetic stirrer. Separately, 0.25 g of Pluronic F127 was dissolved in 3 mL of ethanol in a 50 mL beaker by stirring for 20 min to ensure complete dissolution. Pluronic F127 acts as a soft template to create porosity in the silica matrix (Fig. 3) [40,41].

The surfactant solution was then added to the ethanol-water mixture, followed by 5 mL of TEOS and sufficient hydrochloric acid to reduce the pH to 2. The sol was stirred for 60 min to ensure thorough hydrolysis and uniform nanoparticle formation. pH measurements were taken using multiple types of pH paper to ensure accuracy, by rubbing a glass rod tip dipped in the sol onto the pH paper. To study the effect of porosity, three sols were prepared by varying only the amount of Pluronic F127 with 0.25 g, 0.40 g, or 0.60 g of this chemical. After aging for 24 h, the acid- and base-catalysed sols were mixed to form a stable hybrid sol suitable for coating.

The resulting silica sol was deposited onto low-iron soda lime glass substrates purchased from SUIMA (China) with a thickness of 1 mm and a diameter of 30 mm. Substrates were thoroughly cleaned with ethanol and allowed to dry prior to coating to ensure adhesion and uniformity. For spin coating, approximately 0.5 mL of sol was dispensed onto the substrate. The spin-coating process was performed in two stages: an initial spread at 500 rpm to ensure uniform dispersion (dynamic coating), followed by spinning at 1500 rpm for 20 s to achieve the desired film thickness of ~200 nm. This coating process is repeated one, two, and three times, with a 5-min ambient drying period between each cycle, to fabricate coatings with different thicknesses. The resulting samples are referred to as single-layer, double-layer, and triple-layer coatings. It should be noted that partial re-dissolution of the previously deposited layer can occur during repeated coating. Therefore, the detailed coating thicknesses should be determined from the SEM images presented in the following sections. Following deposition, all coated substrates were sintered in a microwave furnace at 450 °C for 1 h. Sintering facilitated the removal of organic components such as Pluronic F127 and enhanced the structural integrity and optical properties of the porous silica coatings (Fig. 3).

2.3. Optical characterisation methods

The optical properties of the fabricated coatings were characterised using ultraviolet-visible-near-infrared (UV-vis-NIR) spectrophotometry (Cary 7000 UV-Vis-NIR by Agilent) and Fourier transform infrared (FTIR) spectroscopy (Vertex 70, with a A562 Integrating Sphere by Bruker Optik GmbH, Germany). Spectrophotometry was used to measure the transmittance and reflectance of the coatings across the solar spectrum range (300-1200 nm), enabling assessment of their anti-reflective performance. FTIR was employed to evaluate the thermal emissive properties of the coatings in the MIR region, particularly within the 8-13 μm atmospheric transparency window relevant for radiative cooling applications. The spectral transmittance $T(\lambda)$ and reflectance $R(\lambda)$ in the mid-infrared range were directly measured by FTIR spectroscopy. The spectral absorptance was then calculated as $A(\lambda) = 1 - T(\lambda) - R(\lambda)$. According to Kirchhoff's law of thermal radiation, the spectral emissivity is equal to the spectral absorptance at thermal equilibrium, i.e., $\varepsilon(\lambda) = A(\lambda)$. Therefore, the emissivity values reported in this study were obtained from the FTIR-measured optical data and averaged over the atmospheric transparency window of 8–13 μm. In addition, scanning electron microscopy (SEM, supra 60 VP, ZEISS, Germany) was used to analyse the surface morphology of the coatings. SEM provided detailed information on particle size, shape, porosity, and film thickness. These observations were essential in confirming the formation of a porous silica network and in correlating the microstructure with the coatings' optical performance.

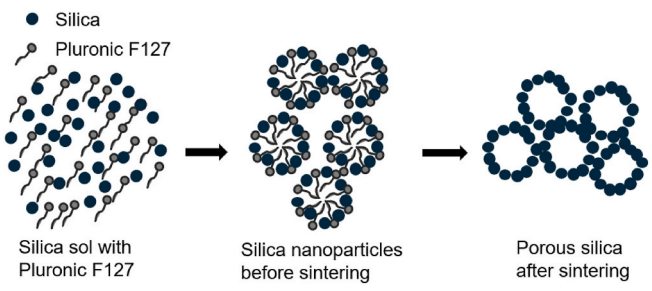

Fig. 3. Mechanism by which Pluronic F127 generates porosity in silica particles.

3. Results and discussions

3.1. Optical performance of the porous silica coatings

The optical performance of porous silica coatings varied with the number of coating layers. The layer number in this study means the times of the spin coating process (e.g., 3-layer coatings means that the substrate is coating three times via the same aforementioned setting of the spin coater). The FTIR and UV-vis-NIR data for coatings fabricated using sols containing 0.25 g of Pluronic F127 are presented in Fig. 4. These include single-layer, double-layer, and triple-layer coatings applied to low-iron soda-lime glass substrates. The optical properties of the soda-lime glass substrate are shown in Fig. 4a as a reference. The transmittance (300-1200 nm, active spectrum for common Si solar cells) and emissivity (8-13 μm) of the soda-lime glass are 89.8% and 87%, respectively. As shown in Fig. 4b, the single-layer porous silica coating exhibited the highest transmittance across the solar spectrum range (300-1200 nm) which reaches 90.9%, compared to the two-layer (Fig. 4c) and three-layer coatings (Fig. 4d). The emissivity (8–13 μm) of the single-layer porous silica coating is 89%. In contrast, as the number of coating layers increased, transmittance decreased, while emissivity in the mid-infrared range (8-13 μm) increased.

Specifically, the three-layer coating, fabricated from the sol containing 0.25 g of Pluronic F127, achieved the highest MIR emissivity, reaching 0.96 (Fig. 4d). This represents an ~10% relative improvement compared to the uncoated glass substrate. The enhancement in emissivity with increasing coating layers can be attributed to the increased mid-infrared optical thickness of the porous silica film. Silica exhibits strong vibrational absorption in the mid-infrared region, mainly associated with Si-O-Si stretching and bending modes. As the number of coating layers increases, the amount of silica interacting with thermal radiation becomes larger, leading to a longer effective optical path length and stronger absorption within the 8-13 μm atmospheric window. According to Kirchhoff's law, this increased mid-infrared absorptance corresponds to higher emissivity. Therefore, the multi-layer porous silica coatings show enhanced thermal emission compared with the single-layer coating and bare glass. These results demonstrate a clear trade-off between optical transparency and radiative cooling potential. A single-layer coating maximises transmittance and is thus suitable for applications prioritising light harvesting (e.g., PV modules), whereas multi-layer coatings enhance emissivity and are more suitable where thermal regulation is prioritised.

The average transmittance (300–1200 nm) for the 1-layer, 2-layer, and 3-layer coatings is 90.9%, 90.4%, and 88.7%, respectively. Compared with bare glass (89.8%), the single-layer and two-layer coatings show absolute improvements of +1.1% and +0.6%. In contrast, the three-layer coating exhibits a slight reduction of −1.1% compared to glass, indicating that excessive layering begins to offset the anti-reflective benefit. The decrease in transmittance with increasing coating layers can be attributed to enhanced optical scattering within the porous silica network. Repeated spin-coating introduces additional nanoparticle interfaces that serve as scattering centres. Given the nanoparticle diameter (~62 nm, as shown in the next section), which is significantly smaller than visible wavelengths, the system operates predominantly in the Rayleigh scattering regime. In this regime, the scattering efficiency increases strongly toward shorter wavelengths

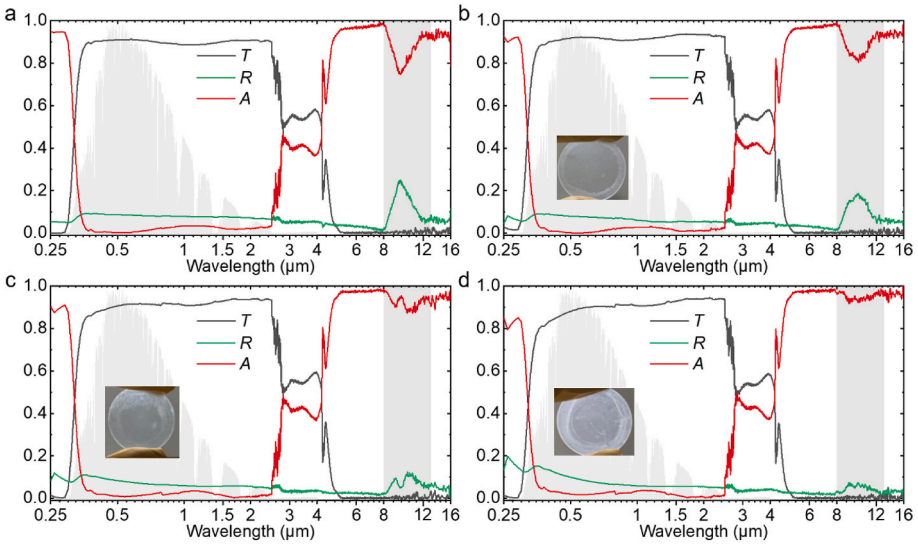

Fig. 4. Optical properties of uncoated and coated soda-lime glass substrates with sample photos. a) Uncoated glass; b) 1-layer porous silica coating; c) 2-layer porous silica coating; d) 3-layer porous silica coating. All coatings were fabricated using 0.25 g of Pluronic F127.

(following a λ^{-4} dependence), making transmission losses more pronounced in the short-wavelength region of the solar spectrum. This behaviour is consistent with the greater reduction in transmittance observed below ~550 nm for the 3-layer porous silica coating as shown in Fig. 4d. In addition, successive deposition on an already porous surface can cause partial pore shrinkage or overlap during drying and sintering, resulting in local densification and slight increases in the effective refractive index.

The mid-infrared emissivity increases from 89% for the single-layer coating to 93% and 96% for the two- and three-layer coatings, respectively, indicating enhanced thermal radiation with increasing layer number. Compared with bare glass, this corresponds to absolute enhancements of +0.01, +0.06, and +0.09, representing relative increases of approximately 1%, 6.9%, and 10.3%, respectively. The increase in emissivity within the 8–13 μm atmospheric window with increasing coating layers is primarily attributed to the intrinsic vibrational modes of the silica network. As the coating thickness increases, the effective optical path length within the silica layer becomes larger, enhancing

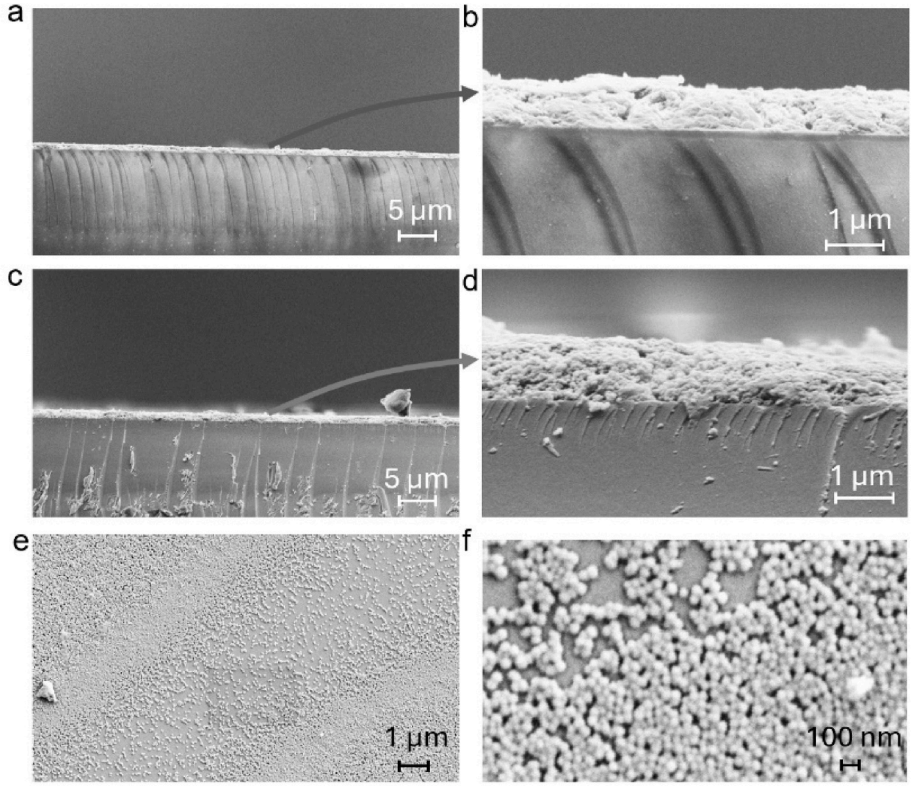

Fig. 5. SEM images of glass substrates coated with porous silica (used 0.25 g Pluronic F127). a) Side view of the 1-layer coating; b) Enlarged side view of the 1-layer coating; c) Side view of the 3-layer coating; d) Enlarged side view of the 3-layer coating; e) Plan SEM view of the 1-layer porous silica coating; f) Enlarged top view of the 1-layer porous silica coating.

absorption of mid-infrared radiation through these vibrational modes. According to Kirchhoff's law of thermal radiation, an increase in absorptivity at a given wavelength corresponds to an increase in emissivity. Therefore, the higher silica content in multi-layer coatings leads to stronger mid-infrared absorption and consequently improved thermal emission within the 8–13 μm range.

3.2. Structure of the porous silica coating

The surface morphology and structural characteristics of the porous silica coatings were examined using SEM, as presented in Fig. 5. The SEM images reveal that the coatings exhibit a uniform and continuous surface, indicating successful deposition and good adhesion to the glass substrate.

The cross-sectional SEM images indicate that the porous silica layer was successfully deposited on the glass substrate. The silica nanoparticles synthesised with 0.25 g of Pluronic F127 were predominantly spherical in shape, with an average particle diameter of ~62 nm, as shown in the plan-view SEM image (Fig. 5e and f). The spherical morphology contributes to the formation of a homogeneous porous network as shown in Fig. 5a–d, which is essential for both anti-reflective and radiative cooling functionalities. The cross-sectional SEM images provide insight into the coating thickness. The coating thickness was determined from cross-sectional SEM images by measuring the vertical distance between the top surface of the porous silica layer and the glass/coating interface at multiple lateral positions. The error bar is reported as the standard deviation of these local thickness measurements. For the single-layer coating, the thickness was measured to be 750 ± 30 nm, while the three-layer coating reached a thickness of 1.14 ± 0.03 μm. The three-layer coating is not three times thicker than the single-layer coating because successive spin-coating does not produce fully discrete layers. During repeated deposition, the freshly applied sol can partially re-dissolve and re-wet the previously deposited porous layer, allowing the solution to infiltrate and fill existing pores rather than forming a purely stacked layer. The layered structure appears compact and well-aligned, suggesting that each subsequent spin-coated layer adheres effectively and contributes to overall film thickness without compromising surface quality. The plan-view SEM images of the 1-layer coating (Fig. 5e and f) show a porous nanoparticle network, but also reveal local inhomogeneity in nanoparticle packing and coverage. This local non-uniformity is likely related to drying-induced redistribution of silica nanoparticles during spin coating, including local de-wetting, particle aggregation, or coffee-ring-like effects during solvent evaporation. Therefore, while the coating is largely continuous at the scale relevant to the optical measurements, further optimization of the sol formulation, substrate surface treatment, spin-coating parameters, and drying conditions will be required to improve microscale coating homogeneity.

Fig. 6 shows the X-ray diffraction patterns of the porous-silica coated glass and the stainless-steel sample holder. The coated sample exhibits a broad diffraction halo between approximately 20° and 35°, which is characteristic of amorphous glass/silica. No additional sharp diffraction peaks associated with crystalline SiO2 phases are observed. The sharp peak at ~43° also appears in the stainless-steel sample holder reference and is therefore attributed to the sample holder/background rather than to the porous silica coating. These results indicate that the sol-gel-derived porous silica coating remains predominantly amorphous after sintering at 450 °C.

3.3. Impact of Pluronic F127 concentration on coating performance

Pluronic F127 was used as a templating agent during the sol-gel synthesis of silica, with the goal of producing coatings with tuneable porosity. Coatings were fabricated from sols containing different amounts of Pluronic F127 (0.25 g, 0.40 g, or 0.60 g), while all other synthesis parameters were kept constant. This allowed investigation of how porosity -induced by varying surfactant content — affects both optical transmittance and thermal emissivity.

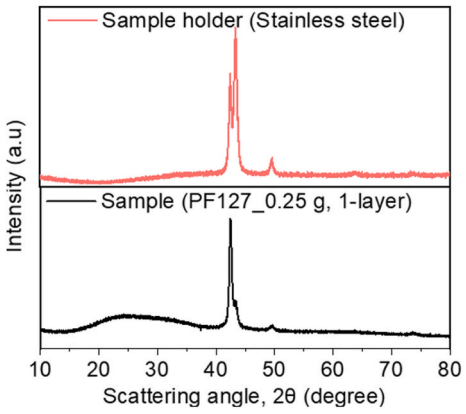

Fig. 6. X-ray diffraction patterns of the porous-silica coated glass sample and the stainless-steel sample holder. The sharp peak at ~43° originates from the stainless-steel holder/background.

Fig. 7 presents the transmittance and emissivity of coatings prepared with 0.40 g of Pluronic F127. The average solar transmittance (300–1200 nm) for the 1-layer, 2-layer, and 3-layer coatings is 91.0%, 91.0%, and 90.2%, respectively. The corresponding mid-infrared emissivity values are 88%, 90%, and 91%. Compared with bare glass (transmittance 89.8% and emissivity 87%), the single- and two-layer coatings exhibit an absolute transmittance enhancement of +1.2%, while the three-layer coating shows a smaller gain of +0.4%. In terms of thermal radiation, the emissivity increases by +0.01, +0.03, and +0.04 for the 1-, 2-, and 3-layer coatings (relatively +1.1%, 3.4%, and 4.6% respectively). The results still indicate an inherent trade-off between maintaining high solar transparency and improving radiative cooling performance. For the coatings prepared with 0.40 g Pluronic F127, the 2-layer coating provides the best balance between solar transmittance and mid-infrared emissivity, as it maintains high solar transparency while improving radiative cooling performance compared with the 1-layer coating. In thicker coatings, incident light travels through a longer porous nanoparticle network. This increases the scattering optical depth and reduces the transmitted light intensity. Because the silica nanoparticles are much smaller than the visible wavelengths, the scattering is stronger at shorter wavelengths, following a Rayleigh-like wavelength dependence. This explains why the transmittance reduction is more pronounced in the short-wavelength region for thicker porous-silica coatings. In addition, when the coating becomes too thick, the anti-reflective condition is no longer optimized, which can further reduce the transmittance.

To isolate the influence of Pluronic F127 concentration, Fig. 8 compares single-layer coatings prepared from sols containing 0.25 g, 0.40 g, and 0.60 g of F127. A single-layer configuration was selected because the previous results demonstrate that it provides the highest

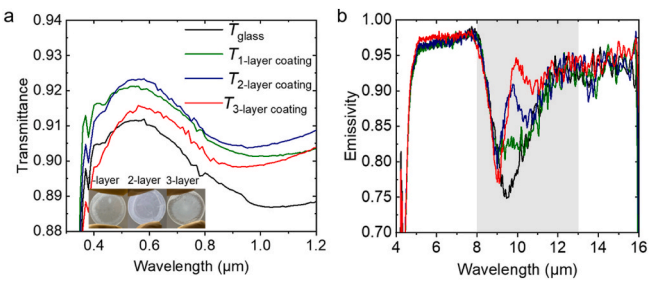

Fig. 7. Optical properties (transmittance and emissivity) of 1-, 2-, and 3-layer coatings fabricated from a sol containing 0.40 g of Pluronic F127.

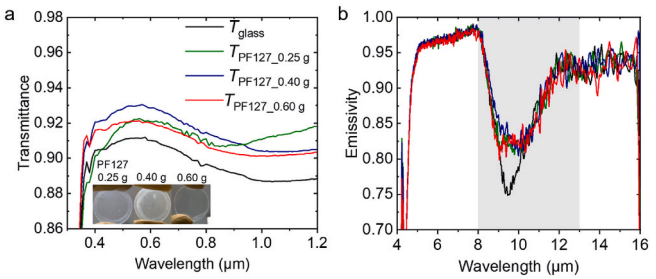

Fig. 8. Comparison of 1-layer porous silica coatings fabricated with 0.25 g, 0.40 g, or 0.60 g of Pluronic F127: a) Transmittance across the 300–1200 nm range; b) Emissivity in the 8-13 μm range.

solar transmittance (300–1200 nm), which is critical for maximizing photon flux to the underlying solar cell. The average solar transmittance (300–1200 nm) for the coatings prepared with 0.25 g, 0.40 g, and 0.60 g of F127 is 90.9%, 91.0%, and 91.0%, respectively, while the corresponding emissivity values are the same of 89%. Within this concentration range, both the optical transmission and mid-infrared emissivity remain nearly unchanged. This limited variation suggests that, for a single-layer coating, increasing the F127 content from 0.25 g to 0.60 g does not significantly alter the effective refractive index or the overall porosity of the silica network (in 300-1200 nm range). Although higher F127 loading can promote pore formation during template removal, the resulting structural changes appear to be moderate. Similarly, the total silica content and vibrational absorption bands responsible for mid-infrared emission remain comparable, leading to only marginal differences in emissivity.

The correlation between Pluronic content and film thickness is shown SEM cross-sectional images in Fig. 9. One-layer coatings fabricated with 0.25 g, 0.40 g, and 0.60 g of Pluronic F127 yielded average thicknesses of 750 ± 30 nm, 310 ± 20 nm, and 200 ± 10 nm, respectively. Similarly, triple-layer coatings reached 1.30 ± 0.03 μm (0.40 g Pluronic F127) and 960 ± 30 nm (0.60 g Pluronic F127). Since, Pluronic F127 is a triblock copolymer (PEO-PPO-PEO) that self-assembles into micelles in aqueous solution [42], when it is used as a template in silica sol-gel, Pluronic F127 micelles direct the formation of mesoporous silica structures. The concentration of Pluronic F127 influences the size, packing, and number of these micelles, which in turn affects the morphology and thickness of the resulting silica coating. The thick hydrophilic PEO shell of Pluronic F127 micelles provides steric

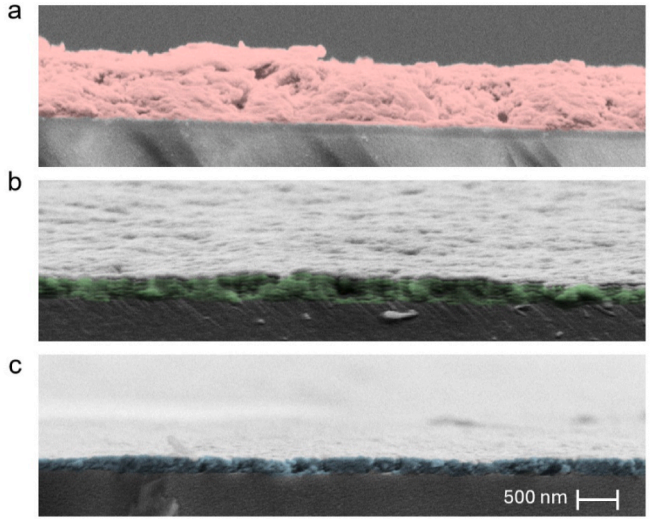

Fig. 9. SEM side-view images of 1-layer coatings fabricated using different amounts of Pluronic F127: a) 0.25 g, b) 0.40 g, c) 0.60 g. Coloured highlights indicate coating thickness.

stabilisation. Furthermore, increasing the Pluronic F127/silica ratio can initially increase pore size, but when the template dominates, the silica walls between pores become thinner, and the overall coating thickness decreases [43]. It should be noted that the present SEM characterization provides information on the coating morphology and thickness. Direct quantitative porosity analysis would require additional techniques, such as ellipsometric porosimetry and nitrogen adsorption measurements. Therefore, in this study, the effect of Pluronic F127 content is evaluated through changes in coating thickness, morphology, and optical performance. The nearly unchanged transmittance and emissivity for the single-layer coatings suggest that, within the investigated F127 range, the effective optical porosity does not change strongly enough to significantly affect the measured optical response.

4. Conclusion

Porous silica coatings were fabricated via a Pluronic F127-assisted sol–gel process and deposited on low-iron soda-lime glass using repeated spin coating. The optical and thermal performance of the coatings was systematically evaluated as a function of layer number and surfactant concentration. The optimal coating configuration depends on the Pluronic F127 content and the relative importance of solar transmittance and mid-infrared emissivity. For coatings fabricated with 0.25 g Pluronic F127, the single-layer coating achieves the highest solar transmittance of 90.9%, with an emissivity of 89%. In contrast, for coatings fabricated with 0.40 g Pluronic F127, the 2-layer coating provides the best balance, as it maintains similarly high solar transmittance of 91.0% while offering higher mid-infrared emissivity of 90%. Increasing the number of layers progressively enhanced emissivity (up to 96%, ~10% relative improvement over glass) due to increased silica optical thickness and stronger Si–O–Si vibrational absorption. However, additional layers introduced enhanced Rayleigh-type scattering and slight structural densification, leading to reduced solar transmittance, particularly at shorter wavelengths. In contrast, varying the Pluronic F127 concentration between 0.25 g and 0.60 g had only a minor influence on the optical performance of single-layer coatings, despite affecting film thickness. This suggests that within the investigated range, surfactant concentration plays a secondary role in determining the transparency–emissivity trade-off compared with coating thickness (layer number). Overall, the study clarifies the competing effects between optical transparency and radiative cooling performance in porous silica coatings and identifies layer number as the primary tuning parameter for balancing these properties.

In this study, spin coating is used because it provides good control over coating thickness and uniformity, while being simple and convenient for laboratory-scale sample preparation. However, spin coating is intrinsically limited to small-area substrates and is not directly suitable for large-area PV cover glass or industrial module-scale fabrication. For future large-area applications, scalable methods such as dip coating, spray coating, slot-die coating, blade/bar coating, or roll coating should be considered. In these processes, the final thickness can be controlled by parameters such as sol viscosity, coating speed, withdrawal speed, wet-film thickness, solvent evaporation rate, and post-treatment conditions. Since the optical transmittance and mid-infrared emissivity are strongly affected by coating thickness, maintaining thickness uniformity over large areas will be a key challenge. Therefore, future work should focus on translating the present spin-coated laboratory films to scalable deposition routes with improved thickness control and large-area uniformity.

From the perspective of PV performance, the most relevant result is that the single-layer porous silica coating increases the average solar transmittance from 89.8% for bare glass to about 91.0%, corresponding to an absolute increase of ~1.2%. If applied to PV cover glass, this higher transmittance can directly increase the photon flux reaching the solar cells and therefore contribute to a modest increase in power output. Assuming that the photocurrent scales approximately linearly with

transmitted solar irradiance, a PV module with an efficiency of 20% could show an absolute efficiency increase of approximately 0.25%, reaching ~20.25%, from this optical gain alone. At the same time, the slightly enhanced mid-infrared emissivity may promote radiative heat dissipation and help reduce the operating temperature of the PV module, providing an additional cooling-related benefit. However, the actual net gain will depend on module design and outdoor conditions, including irradiance, ambient temperature, wind speed, mounting configuration, and the temperature coefficient of the PV module, which is around −0.26%/°C for commercial silicon PV modules (e.g., LONGi Hi-Mo X10). Therefore, future work should integrate the coating with operational PV modules and evaluate the electrical performance gain under real outdoor conditions.

Future work should focus on improving the balance between solar transmittance and mid-infrared emissivity by refining the coating microstructure. In particular, controlling nanoparticle size distribution and pore uniformity may help reduce short-wavelength Rayleigh scattering while maintaining high infrared absorption. The development of graded-refractive-index or thickness-optimized architectures could further enhance impedance matching across the solar spectrum without sacrificing radiative cooling performance. Finally, integration of the coatings with operational photovoltaic devices under real outdoor conditions will be necessary to quantify the net impact on electrical efficiency and temperature reduction. In addition, the anti-soiling potential of the porous silica coating should also be investigated, as dust accumulation is an important factor affecting the long-term performance of PV modules. Furthermore, scalable large-area deposition methods, such as dip coating, spray coating, slot-die coating, blade/bar coating, or roll coating, should be developed to facilitate industrial application on PV cover glass.

CRediT authorship contribution statement

Leonard E. Namwiha: Conceptualization, Formal analysis, Investigation, Methodology, Validation, Visualization, Writing – original draft, Writing – review & editing. **Markus Guttmann:** Investigation, Methodology, Writing – review & editing. **Marco Ehrhardt:** Investigation, Methodology. **Tonghan Zhao:** Investigation, Methodology. **Bryce S. Richards:** Conceptualization, Formal analysis, Funding acquisition, Investigation, Methodology, Supervision, Writing – original draft, Writing – review & editing. **Gan Huang:** Conceptualization, Formal analysis, Funding acquisition, Investigation, Methodology, Project administration, Resources, Supervision, Visualization, Writing – original draft, Writing – review & editing.

Declaration of competing interests

The authors declare that they have no known competing financial interests or personal relationships that could have appeared to influence the work reported in this paper.

Acknowledgements

L.E.N thanks the support from Southern African Science Service Centre for Climate Change and Adaptive Land Management (SASSCAL), the Federal Ministry of Education and Research (BMBF). G.H. and B.S.R. gratefully acknowledge financial support received from: i) KIT YIG-Prep-Pro project (G.H.); ii) the Helmholtz Association Research Field Energy: Program Materials and Technologies for the Energy Transition (Topic 1 Photovoltaics and Wind Energy, ref. 38.01.04) (B.S.R.); iii) the Karlsruhe School of Optics and Photonics (KSOP) (G.H. and B.S.R.); and iv) Initiative and Networking Fund of the Helmholtz Association under the call Helmholtz Investigator Group (VH-NG-21-07, UNICOS) (G.H.)

Data availability

Data will be made available on request.

References

[1] K. Hasan, S.B. Yousuf, M.S.H.K. Tushar, B.K. Das, P. Das, M.S. Islam, Effects of Different Environmental and Operational Factors on the PV Performance: a Comprehensive Review, John Wiley and Sons Ltd, Feb. 01, 2022, https://doi.org/10.1002/ese3.1043.

[2] A.M. Law, L.O. Jones, J.M. Walls, The Performance and Durability of Anti-reflection Coatings for Solar Module Cover Glass – a Review, Elsevier Ltd., Sep. 01, 2023, https://doi.org/10.1016/j.solener.2023.06.009.

[3] A. Shukla, K. Kant, A. Sharma, P.H. Biwole, Cooling methodologies of photovoltaic module for enhancing electrical efficiency: a review, Sol. Energy Mater. Sol. Cell. 160 (Feb. 2017) 275–286, https://doi.org/10.1016/J.SOLMAT.2016.10.047.

[4] ANERN store, Ultimate Guide to PERC, TOPCon, and HJT modules for 2025. https://www.anernstore.com/blogs/diy-solar-guides/perc-topcon-hjt-guide-2025?srsltid=AfmBOorNVppIiinclt1XnNh0ud2TvI_yYLO0lCzrLjrFv7y4EPpirNlf. (Accessed 16 December 2025).

[5] M.M. Rahman, M. Hasanuzzaman, N.A. Rahim, Effects of various parameters on PV-module power and efficiency, Energy Convers. Manag. 103 (Jul. 2015) 348–358, https://doi.org/10.1016/j.enconman.2015.06.067.

[6] N. Shanmugam, R. Pugazhendhi, R.M. Elavarasan, P. Kasiviswanathan, N. Das, Anti-reflective coating materials: a holistic review from PV perspective, Energies (Basel) 13 (10) (May 2020), https://doi.org/10.3390/en13102631.

[7] E. Enasel, A.-G. Lupu, G. Dumitrascu, Design and development of cooling systems for PV cells performance improvement, Bull. Polytech. Inst. Iasi. Machine C onstruct Section 69 (2) (Jun. 2023) 71–84, https://doi.org/10.2478/bipcm-2023-0016.

[8] Natarajan Shanmugam, Rishi Pugazhendhi, Rajvikram Madurai Elavarasan, Pitchandi Kasiviswanathan, Narottam Das, Anti-reflective coating materials: a holistic review from PV perspective, Energies 13 (10) (2020) 2631.

[9] Chih-Hung Sun, Peng Jiang, Bin Jiang, Broadband moth-eye antireflection coatings on silicon, Appl. Phys. Lett. 92 (6) (2008).

[10] Gan Huang, Ashok R. Yengannagari, Kishin Matsumori, Prit Patel, Anurag Datla, Karina Trindade, Enkhlen Amarsanaa, et al., Radiative cooling and indoor light management enabled by a transparent and self-cleaning polymer-based metamaterial, Nat. Commun. 15 (1) (2024) 3798.

[11] Aiman Roslizar, Stephan Dottermusch, Raphael Schmager, Markus Guttmann, Guillaume Gomard, Hendrik Hölscher, Bryce S. Richards, Ulrich W. Paetzold, Hot-embossed microcone-textured fluoropolymer as self-cleaning and anti-reflective photovoltaic module covers, Sol. Energy Mater. Sol. Cell. 214 (2020) 110582.

[12] M.A. Zahid, M. de Assis Rabelo, H. Yousuf, Y. Kim, D.P. Pham, J. Yi, Anti-reflective coating and cooling technique for innovative photovoltaic system in tropical region, J. Power Sources 564 (Apr. 2023), https://doi.org/10.1016/j.jpowsour.2023.232812.

[13] M. Chen, D. Pang, X. Chen, H. Yan, Y. Yang, Passive daytime radiative cooling: fundamentals, material designs, and applications, EcoMat 4 (1) (Jan. 2022) e12153, https://doi.org/10.1002/EOM2.12153.

[14] J. Liu, et al., Passive photovoltaic cooling: advances toward low-temperature operation, Adv. Energy Mater. 14 (2) (Jan. 2024), https://doi.org/10.1002/AENM.202302662.

[15] E.B. Agyekum, S. Praveenkumar, N.T. Alwan, V.I. Velkin, S.E. Shcheklein, S. J. Yaqoob, Experimental investigation of the effect of a combination of active and passive cooling mechanism on the thermal characteristics and efficiency of solar PV module, Inventions 6 (4) (Oct. 2021) 63, https://doi.org/10.3390/INVENTIONS6040063, 2021, Vol. 6, Page 63.

[16] M. Huang, H. Zhou, G.H. Tang, M. Du, Q. Sun, The potential of radiative cooling enhanced photovoltaic systems in China, Adv. Appl. Energy 15 (2024) 100184.

[17] S. Zhang, P. Xiao, P. Wang, J. Luo, B. Jiang, Spherical-chain silica with super-hydrophobic surface and ultra-low refractive index for multi-functional broadband antireflective coatings, Sol. Energy 207 (Sep. 2020) 1222–1230, https://doi.org/10.1016/J.SOLENER.2020.05.060.

[18] A. Kumar, A. Chowdhury, Effect of multilayer selective radiative anti-reflective coating on crystalline silicon photovoltaics for operating temperature reduction, Int. J. Sustain. Energy (2020) 982–996, https://doi.org/10.1080/14786451.2020.1785466.

[19] B. McLean, I. Yarovsky, Structure, properties, and applications of silica nanoparticles: recent theoretical modeling advances, challenges, and future directions, Small (Dec. 2024), https://doi.org/10.1002/SMLL.202405299.

[20] R. Liu, S. Wang, Z. Zhou, K. Zhang, G. Wang, C. Chen, Y. Long, Materials in radiative cooling technologies, Adv. Mater. 37 (2) (2025) 2401577.

[21] R. Ciriminna, A. Fidalgo, V. Pandarus, F. Béland, L.M. Ilharco, M. Pagliaro, The sol-gel route to advanced silica-based materials and recent applications, Chem. Rev. 113 (8) (Aug. 2013) 6592–6620, https://doi.org/10.1021/CR300399C/ASSET/IMAGES/MEDIUM/CR-2012-00399C_0031.GIF.

[22] S. Cai, Y. Zhang, H. Zhang †, H. Yan, H. Lv, and B. Jiang, "Sol-Gel Preparation of Hydrophobic Silica Antireflective Coatings with Low Refractive Index by base/acid Two Step Catalysis.".

[23] X. Wang, A. Catalogue, W. Key, Preparation, synthesis and application of Sol-gel method [Online]. Available: https://www.researchgate.net/publication/344942631.

[24] A.E. Danks, S.R. Hall, Z. Schnepp, The evolution of 'sol–gel' chemistry as a technique for materials synthesis, Mater. Horiz. 3 (2) (Feb. 2016) 91–112, https://doi.org/10.1039/C5MH00260E.
[25] N. Nuraje, K. Su, H. Matsui, Catalytic growth of silica nanoparticles in controlled shapes at planar liquid/liquid interfaces, New J. Chem. 31 (11) (2007) 1895, https://doi.org/10.1039/B712260H.
[26] F. Rizzi, et al., High surface area mesoporous silica nanoparticles with tunable size in the sub-micrometer regime: insights on the size and porosity control mechanisms, Molecules 26 (14) (Jul. 2021) 4247, https://doi.org/10.3390/MOLECULES26144247.
[27] L. Zou, X. Li, Q. Zhang, J. Shen, An abrasion-resistant and broadband antireflective silica coating by block copolymer assisted sol-gel method, Langmuir 30 (34) (Sep. 2014) 10481–10486, https://doi.org/10.1021/la502397e.
[28] M. Faustini, B. Louis, P.A. Albouy, M. Kuemmel, D. Grosso, Preparation of sol-gel films by dip-coating in extreme conditions, J. Phys. Chem. C 114 (17) (May 2010) 7637–7645, https://doi.org/10.1021/jp9114755.
[29] L.E. Scriven, Physics and applications of DIP coating and spin coating, MRS Proceed. 121 (1) (Feb. 1988) 717–729, https://doi.org/10.1557/PROC-121-717/METRICS.
[30] W. Zhang, J. Tu, W. Long, W. Lai, Y. Sheng, T. Guo, Preparation of SiO2 anti-reflection coatings by sol-gel method, Energy Proc. 130 (2017) 72–76.
[31] D. Chen, Anti-reflection (AR) coatings made by sol–gel processes: a review, Sol. Energy Mater. Sol. Cell. 68 (3–4) (2001) 313–336.
[32] B. Ma, Y. Cheng, P. Hu, D. Fang, J. Wang, Passive daytime radiative cooling of silica aerogels, Nanomaterials 13 (3) (2023) 467.
[33] D. Han, C. Wang, C.B. Han, Y. Cui, W.R. Ren, W.K. Zhao, H. Yan, Highly optically selective and thermally insulating porous calcium silicate composite SiO2 aerogel coating for daytime radiative cooling, ACS Appl. Mater. Interfaces 16 (7) (2024) 9303–9312.
[34] L. Long, Y. Yang, L. Wang, Simultaneously enhanced solar absorption and radiative cooling with thin silica micro-grating coatings for silicon solar cells, Sol. Energy Mater. Sol. Cell. 197 (2019) 19–24.
[35] Y. Lu, Z. Chen, L. Ai, X. Zhang, J. Zhang, J. Li, W. Song, A universal route to realize radiative cooling and light management in photovoltaic modules, Sol. RRL 1 (10) (2017) 1700084.
[36] S. Cai, Y. Zhang, H. Zhang, H. Yan, H. Lv, B. Jiang, Sol-gel preparation of hydrophobic silica antireflective coatings with low refractive index by base/acid two-step catalysis, ACS Appl. Mater. Interfaces 6 (14) (Jul. 2014) 11470–11475, https://doi.org/10.1021/AM501972Y/SUPPL_FILE/AM501972Y_SI_001.PDF.
[37] H. Ye, et al., Preparation of antireflective coatings with high transmittance and enhanced abrasion-resistance by a base/acid two-step catalyzed sol-gel process, Sol. Energy Mater. Sol. Cell. 95 (8) (Aug. 2011) 2347–2351, https://doi.org/10.1016/j.solmat.2011.04.004.
[38] S. Cai, Y. Zhang, H. Zhang, H. Yan, H. Lv, B. Jiang, Sol-gel preparation of hydrophobic silica antireflective coatings with low refractive index by base/acid two-step catalysis, ACS Appl. Mater. Interfaces 6 (14) (Jul. 2014) 11470–11475, https://doi.org/10.1021/AM501972Y.
[39] R. Ciriminna, M. Sciortino, G. Alonzo, A. De Schrijver, M. Pagliaro, From molecules to systems: sol-gel microencapsulation in silica-based materials, Chem. Rev. 111 (2) (Feb. 2011) 765–789, https://doi.org/10.1021/CR100161X/ASSET/IMAGES/MEDIUM/CR-2010-00161X_0041.GIF.
[40] A.G. Morozov, et al., Deposition of silicon dioxide antireflection coatings on glass by sol-gel method in the presence of pluronic® F127 block-copolymer, Russ. J. Appl. Chem. 89 (1) (Jan. 2016) 108–113, https://doi.org/10.1134/S1070427216010171.
[41] S. Ramakrishnan, S. Jayaraj, C.N. Ragupathy, Investigation of photocatalytic performance of single layer superhydrophilic film: TEOS/PF-127, Environ. Qual. Manag. 33 (4) (Jun. 2024) 705–711, https://doi.org/10.1002/tqem.22146.
[42] S. Kerkhofs, et al., Self-assembly of pluronic F127 - silica spherical core-shell nanoparticles in cubic close-packed structures, Chem. Mater. 27 (15) (Aug. 2015) 5161–5169, https://doi.org/10.1021/ACS.CHEMMATER.5B01772/SUPPL_FILE/CM5B01772_SI_003.MPG.
[43] D.R. Dunphy, P.H. Sheth, F.L. Garcia, C.J. Brinker, Enlarged pore size in mesoporous silica films templated by pluronic F127: use of poloxamer mixtures and increased template/SiO2 ratios in materials synthesized by evaporation-induced self-assembly, Chem. Mater. 27 (1) (Jan. 2015) 75–84, https://doi.org/10.1021/cm5031624.